Hypoxia triggers collective aerotactic migration in *Dictyostelium discoideum*

O. Cochet-Escartin[1]*, M. Demircigil[2], S. Hirose[3,4], B. Allais[1], V. Calvez[2], K. Funamoto[3,4,5], C. Anjard[1], J.-P. Rieu[1]*

Affiliations:

1-Institut Lumière Matière, UMR5306, Université Lyon 1-CNRS, Université de Lyon, 69622 Villeurbanne, France

2- Institut Camille Jordan, UMR5208, Université Lyon 1-CNRS, Université de Lyon, 69622 Villeurbanne, France

3- Graduate School of Biomedical Engineering, Tohoku University, 6-6-12 Aramaki-aza Aoba, Aoba-ku, Sendai, Miyagi 980-8579, Japan

4- Institute of Fluid Science, Tohoku University, 2-1-1 Katahira, Aoba-ku, Sendai, Miyagi 980-8577, Japan

5- Graduate School of Engineering, Tohoku University, 6-6 Aramaki-aza Aoba, Aoba-ku, Sendai, Miyagi 980-8579, Japan

Keywords: Hypoxia, Self-generated gradients, Chemotaxis, Collective migration, Oxygen sensing

Abstract

It is well known that eukaryotic cells can sense oxygen (O_2) and adapt their metabolism accordingly. It is less known that they can also move towards regions of higher oxygen level (aerotaxis). Using a self-generated hypoxic assay, we show that the social amoeba *Dictyostelium discoideum* displays a spectacular aerotactic behavior. When a cell colony is covered by a coverglass, cells quickly consume the available O_2 and the ones close to the periphery move directionally outward forming a dense ring keeping a constant speed and density. To confirm that O_2 is the main molecular player in this seemingly collective process, we combined two technological developments, porphyrin based O_2 sensing films and microfluidic O_2 gradient generators. We showed that *Dictyostelium* cells exhibit aerotactic and aerokinetic (increased speed at low O_2) response in an extremely low range of O_2 concentration (0-1.5%) indicative of a very efficient detection mechanism. The various cell behaviors under self-generated or imposed O_2 gradients were modeled with a very satisfactory quantitative agreement using an *in silico* cellular Potts model built on experimental observations. This computational model was complemented with a parsimonious 'Go or Grow' partial differential equation (PDE) model. In both models, we found that the collective migration of a dense ring can be explained by the interplay between cell division and the modulation of aerotaxis, without the need for cell-cell communication. Explicit wave solutions of the PDE model also informed about the relative contributions of division and directed motion on the collective speed.

Introduction

Oxygen is the main electron acceptor for aerobic organism to allow efficient ATP synthesis. This high-energy metabolic pathway has contributed to the emergence and diversification of multicellular organism (1). While high O_2 availability in the environment seems a given, its rapid local consumption can generate spatial and temporal gradients in many places, including within multicellular organism. Oxygen level and gradients are increasingly recognized as a central parameter in various physiopathological processes (2). O_2 concentration influences the growth and differentiation of neural and stem cells. The well-known HIF (hypoxia inducible factor) pathway allows cells to regulate their behavior when exposed to hypoxia. The key enzyme PHD2 regulates transcription in metazoa, via an O_2-dependent degradation of the transcriptional co-factor HIFα. At low O_2 levels, cells then

accumulate HIFα leading to the expression of genes that support cell functions appropriate to hypoxia (3).

Another strategy used by organisms facing severe oxygen conditions is to move from hypoxic regions toward an optimal oxygen concentration region, a mechanism called aerotaxis which has long been known in bacteria (4, 5). Aerotaxis will occur at the interface between environments with different oxygen content, such as soil/air, water/air or even within eukaryotic multicellular organisms between different tissue types (6). In eukaryotic multicellular organisms, oxygen was proposed to be a morphogen as in placentation (7) or a chemoattractant during sarcoma cell invasion toward blood vessels (8) but such studies are relatively scarce due to the difficultly to measure oxygen gradients *in vivo*.

Recently, it was demonstrated that after covering an epithelial cell colony by a coverglass non permeable to O_2, peripheral cells exhibit a strong outward directional migration to escape hypoxia from the center of the colony (9). This is a striking example of collective response to a self-generated oxygen gradient. Self-generated chemoattractant gradients have been reported to trigger the dispersion of melanoma cells (10, 11) or *Dictyostelium* cells (12) or the migration of the zebrafish lateral line primordium along a self-generated SDF-1/CXCL12 gradient (13, 14). The mechanism is simple and very robust: the cell colony acts as a sink for the chemoattractant, removes it by degradation or uptake creating a gradient that, in turn, attracts the cells up to very long distances and as long as the chemoattractant is present in the environment.

Dictyostelium discoideum (*Dd*) is an excellent model system to study the still very virgin field of aerotaxis and in particular of self-generated aerotaxis. *Dd* is an obligatory aerobic organism that requires at least 5% O_2 to grow at optimal exponential rate (15, 16) while slower growth can occur at 2% O_2. However, its ecological niche in the soil and around large amount of bacteria can result in reduced O_2 availability. During its multicellular motile stage, high oxygen level is one of the signal used to trigger culmination of the migrating slug (17). *Dd* is a soil amoeba feeding on bacteria and able to chemotax toward folic acid and other molecules released by their preys (18, 19). For many years, *Dd* has been a classical organism to study chemotaxis and has emulated the development of many models of emergent and collective behavior since the seminal work of Keller and Segel (20, 21). An integrated approach combining biological methods (the use of mutants), technological progress (*i.e.*, assays and microsystems), and mathematical modeling (via PDE and computational models) is very valuable to tackle the issue of aerotaxis.

In this article, we study the influence of O_2 self-generated gradients on *Dd* cells. Using first a simple confinement assay, then microfluidic tools, original oxygen sensors and theoretical approaches, we show that oxygen self-generated gradients can direct a seemingly collective migration of a cell colony. Our results confirm the remarkable robustness and long-lasting effect of self-generated gradients in collective migration. This case where oxygen is the key driver also suggests that self-generated gradients are widespread and a possible important feature in multicellular morphogenesis.

Results

Confinement triggers formation and propagation of a self-sustained cell ring. To trigger hypoxia on a colony of *Dd* cells, we used the vertical confinement strategy presented in (9). A spot of cells with a radius of about 1mm was deposited and covered by a larger glass coverslip with a radius of 9mm. We measured the vertical confinement through confocal microscopy and found the typical height between the bottom of the plate and the coverslip to be 50μm (Fig. S1).

This vertical confinement limits the amount of medium immediately available to the cells which can rapidly consume a significant fraction of available nutrients, oxygen etc… As a result, under such vertical confinement, a cell colony can robustly self-generate gradients and can, in turn, respond to these gradients through chemotactic means.

Using spots containing around 2,000 cells (initial density around 10^3 cells/mm^2), the formation of a dense ring of cells moving outwards was observed as quickly as 30min after initiation of the confinement (Fig. 1A and Supplementary movie M1). This formation time however depended non-linearly on initial cell density (the denser, the faster, Fig. S2). Once triggered, this collective migration was self-maintained for tens of hours, even days and the ring could, at these points, span centrimetric distances, orders of magnitude larger than the initial size of the cell spot (Fig. 1B).

Notably, as the ring expanded outwards, it left a trail of cells behind. This led to the formation of a central zone populated by cells which didn't contribute to the collective migration of the ring (Fig. 1B) but were still alive and moving albeit a clear elongated phenotype resembling pre-aggregative *Dd* cells (Fig. 1C and Supplementary movie M2). On the other hand, cells in the ring or outside the colony were rounder, as usual vegetative cells (22).

To study the properties of the ring, we computed density profiles using radial coordinates from the center of the colony to study cell density as a function of time and distance to the center of the colony (Fig. 1D-E). We found that after a transitory period corresponding to the ring passing through the initial spot, the density in the ring, its width and its speed all remained constant over long time scales (Fig. S3). The speed and density of the ring were found to be 1.2 ± 0.3 µm/min (mean±std, N=9) and 1.9 10^3 ± 0.3 10^3 cells/mm^2 (mean±std, N=4, *i.e.*, 4-fold higher than behind it, Fig. 1E) respectively. The density of cells left behind the ring was also found to remain constant after a transient regime (Fig. 1D). As the diameter of the ring increased over time, the absence of changes in morphology has to imply an increase of the number of cells and thus an important role of cell division in this process.

Overall, this self-sustained ring propagation is very robust and a long lasting collective phenotype that can easily be triggered experimentally.

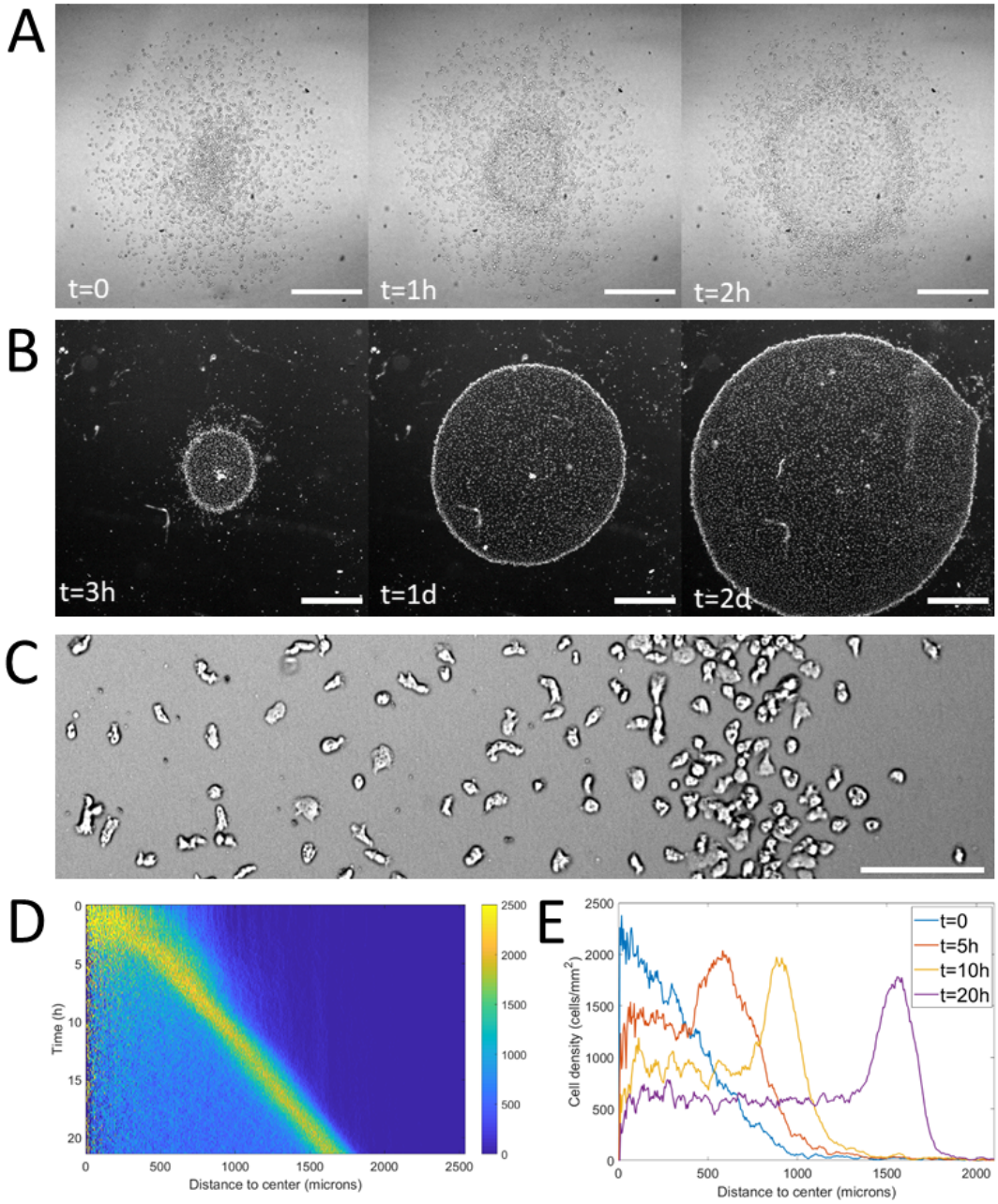

Fig1. *Formation and dynamics of a dense ring of cells after vertical confinement. (A) snapshots of early formation, scale bars: 500μm. (B) snapshots at longer times imaged under a binocular, scale bars: 1mm. (C) close up on a ring already formed moving rightward and showing different cellular shapes in the ring and behind it, scale bar: 100μm. (D) kymograph of cell density over 20h showing the formation and migration of the highly dense ring. (E) Cell density profiles in the radial direction at selected time points.*

Cell dynamics in different regions. Following the reported shape differences, we next questioned how cells behaved dynamically in different regions. To do so, we performed higher resolution, higher frame rate (4 frames per minute) experiments to allow cell tracking over times on the order of tens of minutes. First, we found that both the cell diffusion constant and instantaneous cell speeds were

fairly constant throughout the entire colony (Fig. S4). Cell diffusion was on the order of 28.2 ± 1.4 μm^2/min (N=3), comparable to our measurement of activity at very low oxygen level in the microfluidic device (see below). Then, to test the influence of motion bias, we projected cell displacements on the radial direction and computed mean speeds in this direction as a function of distance to the center. Random motion, either persistent or not, would lead to a null mean radial displacement whereas biased migration would be revealed by positive (outward motion) or negative (inward motion) values. Here, we found that significantly non-zero biases were observed only in a small region spanning the entire ring and a few tens of microns behind and in front of it with the strongest positive biases found in the exact region of the ring (Fig. S5).

Overall, our results show that the different regions defined by the ring and its dynamics can be characterized in terms of cell behavior: (i) behind the ring in the hypoxic region: elongated shape, normal speeds, and low bias; (ii) in the ring: round shape, normal speeds and high bias. We also performed several complementary experiments (replacing the nutritive HL5 medium with a non-nutrient phosphate buffer, pre-treating cells with Ethidium Bromide to reduce their respiration rate and used mutant *Dd* lines overexpressing a superoxide dismutase) that revealed that oxygen depletion is the chemical basis for the apparition and migration of a dense ring of cells (See section 3.1 of supporting information).

Response of *Dd* cells to controlled oxygen gradients. The spot assay is experimentally simple but is not ideally suited to decipher the response of *Dd* cells to hypoxia since local concentrations and gradients of oxygen are intimately linked to cell dynamics and thus very difficult to manipulate. We hence designed a new double-layer PDMS microfluidic device allowing to quickly generate oxygen gradients in a continuous, controlled manner (Fig. 2A). Briefly, cells were seeded homogenously within a media channel positioned 500µm below two gas channels continuously perfused with pure nitrogen on one side and air on the other. As PDMS is permeable to these gases, the gas flows imposed hypoxic conditions on one side of the media channel while the other was kept at atmospheric oxygen concentration. Of note, the distance between the two gas channels, thereafter called the gap, varied from 0.5mm to 2mm in order to modify the steepness of the gradients in the median region of the media channels (details in Fig. 2A caption and in the supporting information).

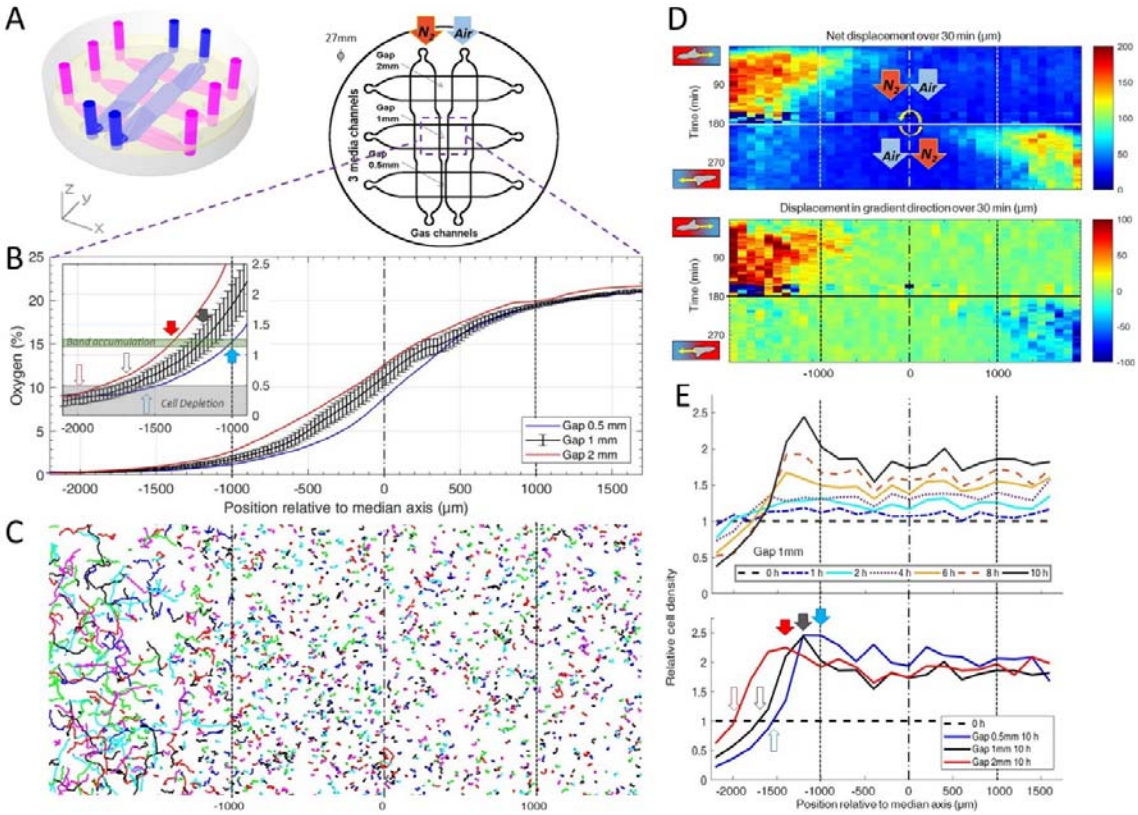

Fig. 2. *Dictyostelium single cells are attracted by an external O_2 gradient when O_2 level drops below 2%. (A) Schemes of the new double-layer PDMS microfluidic device allowing the control of the O_2 gradient by the separation distance (gap) between two gas channels located 0.5 mm above the three media channels. A gas-impermeable polycarbonate film was embedded above the gas channels to avoid O_2 permeation from the top. For this study, we injected pure nitrogen, and air with 21% O_2 to the gas channels. (B) Measured O_2 concentration profiles 30 min after N2-Air injection to the left and right channels respectively (0-21% gradient) as a function of the position along the media channel for the three gaps. Error bars (see supplementary information) are reported only for gap 1 mm for clarity. The inset shows the 0%-2.5% region under the nitrogen gas channel (arrows, see E). (C) Trajectories lasting 1 h between 3h and 4h after establishment of a 0-21% gradient. Cells are fast and directed toward the air side in the region beyond the -1000 µm limit (O_2<2%). (D) Cell net displacement over 30 min (end to end distance, top kymograph) and 30-min displacement projected along gradient direction (bottom kymograph). Cells are fast and directed toward O_2, where O_2<2%, within 15 min after 0-21% gradient establishment at t=0. At t=180 min, the gradient is reversed to 21-0% by permuting gas entries. Cells within 15 min again respond in the 0-2% region. (E) Relative cell density histogram (normalized to t=0 cell density) as a function of the position along media channel. Top panel: long term cell depletion for positions beyond -1600 µm (O_2<0.5%, see inset of B) and resulting accumulation at about -1200 µm for gap 1 mm channel. The overall relative cell density increase is due to cell divisions. Bottom panel: cell depletion and accumulation at 10 h for the three gaps. The empty and filled arrows pointing the limit of the depletion region, and max cell accumulation respectively are reported in the inset of B).*

To make sure that the gas flows were sufficient to maintain a constant O_2 distribution against leakages and against small variation in the fabrication process, we also developed O_2 sensing films to be able to experimentally measure O_2 profiles both in the microfluidic devices and in the spot assay. These films consisted of porphyrin based O_2 sensors embedded in a layer of PDMS. As O_2 gets depleted, the luminescence quenching of the porphyrin complex is reduced leading to an increase in

fluorescence intensity (23). Quantitative oxygen measurements were then extracted from this fluorescent signal using a Stern-Volmer equation (See supporting information and Figs. S9-S12 for details on sensor calibration and O_2 quantification).

First, we observed the formation of a stable O_2 gradient in the devices closely resembling numerical predictions within 15min (Fig. 2B and Fig. S13-14). Then, in the presence of cells seeded at 500 cells/mm^2, we simulated O_2 distribution and exchanges between the various part of the device and showed that cell respiration was more than balanced by the imposed gas flows (Fig. S15).

We then turned our attention to the reaction of the cells to this imposed, stable gradient. We first noticed that depending on local O_2 concentrations, cell motility was remarkably different. Using cell tracking, we could reconstruct cell trajectories and found that these trajectories seemed much longer and more biased in hypoxic regions (Fig. 2C). These aerokinetic and aerotactic responses were confirmed by quantifying the mean absolute distance travelled by cells (Fig. 2D top), or the mean distance projected along the gradient direction (Fig. 2D bottom) in a given time as a function of position in the device (Fig. 2D).

The second important observation stemming from the microfluidic experiments is an accumulation of cells at some midpoint within the cell channel (Fig. 2E). Naively, one could have expected cells to follow the O_2 gradient over its entire span leading to an accumulation of all cells on the O_2 rich side of the channel. This did not happen and, instead, cells seemed to stop responding to the gradient at a certain point. Another way to observe this phenomenon is through the bias in cell motion, *i.e.* the average displacement of cells in the direction of the gradient. We observed a strong positive bias in hypoxic regions but the bias quickly fell to 0 as cells moved to oxygen levels higher than about 2% (Fig. 2D), confirming that the observed cell accumulation was a result of differential migration and not, for example, differential cell division. In addition, if we inverted the gas channels halfway through the experiment, we observed that the cells responded in around 15min (which is also the time needed to re-establish the gradient, see Fig. S14) and showed the same behavior, albeit in reverse positions. We measured this bias (distance travelled along the gradient during 30min) for the different gaps and for the situation of reversed gradient and obtained an average bias speed of 1.1 ± 0.4 µm/min (N=6, three different gaps, each measured in both directions of the gradient).

Of note, the position at which cells accumulated and stopped responding to the gradient was still in the region were the gradient was constantly increasing. This leads to the hypothesis that, in addition to gradient strength, O_2 levels also play an important role in setting the strength of aerotaxis displayed by *Dd* cells.

Furthermore, when we compared experiments performed in the three media channels of the same device with slightly shifted gradient profiles due to gap differences, we found that the position of cell accumulation varied from one channel to another (Fig. 2E). However, our O_2 sensors indicates that the accumulation occurred at a similar O_2 concentration of about 1% in all three channels (inset of Fig. 2B) thus strongly hinting that the parameter controlling the aerotactic response was indeed O_2 levels.

Overall, these experiments in controlled environments demonstrated two main features of the response of *Dd* cells to hypoxia: a strong aerokinetic response (large increase in cell activity) and a positive aerotactic response, both modulated by local O_2 levels regardless of the strength of the local gradient.

In summary, these results reveal a subtle cross talk between O_2 concentrations and gradients in defining cell properties and it would be very informative, in the future, to study in details the reaction of *Dd* cells to various, well defined hypoxic environments where O_2 concentrations and gradients can be independently varied.

Coupled dynamics between oxygen profiles and collective motion. Thanks to these results, we turned our attention back to the collective migration of a ring of cells and asked whether similar

aerotactic behaviors were observed under self-generated gradients. To do so, we performed spot experiments on the O_2 sensing films described above which allowed us to image, in parallel, cell behavior and O_2 distribution (Figs. 3A and S11, Supplementary Movie M3).

In a first phase, preceding the formation of the ring, cell motion was limited and the structure of the colony remained mostly unchanged. As O_2 was consumed by cells, depletion started in the center and sharp gradients appeared at the edges of the colony (Fig. 3B-C).

Then, the ring formed and started moving outwards, O_2 depletion continued and the region of high O_2 gradients naturally started moving outwards (Fig. 3B). At this point, coupled dynamics between the cells and the O_2 distribution appeared and we observed that the position of the ring seemed to closely follow the dynamics of the O_2 field (Fig. 3D). Said differently, we observed that, once formed and after a transitory period, the ring seemed to follow a constant concentration of oxygen of less than 1% (Fig. 3C).

In the process, three distinct regions were created. Behind the ring, O_2 was completely depleted and thus no gradient was visible. In front of the ring, the O_2 concentration remained high with high gradients. Finally, in the ring region, O_2 was low (<1%) and the gradients were strong. Based on our results in externally imposed gradients, we would thus expect cells to present a positive aerotactic bias mostly in the ring region which is indeed what we observed (Fig S5).

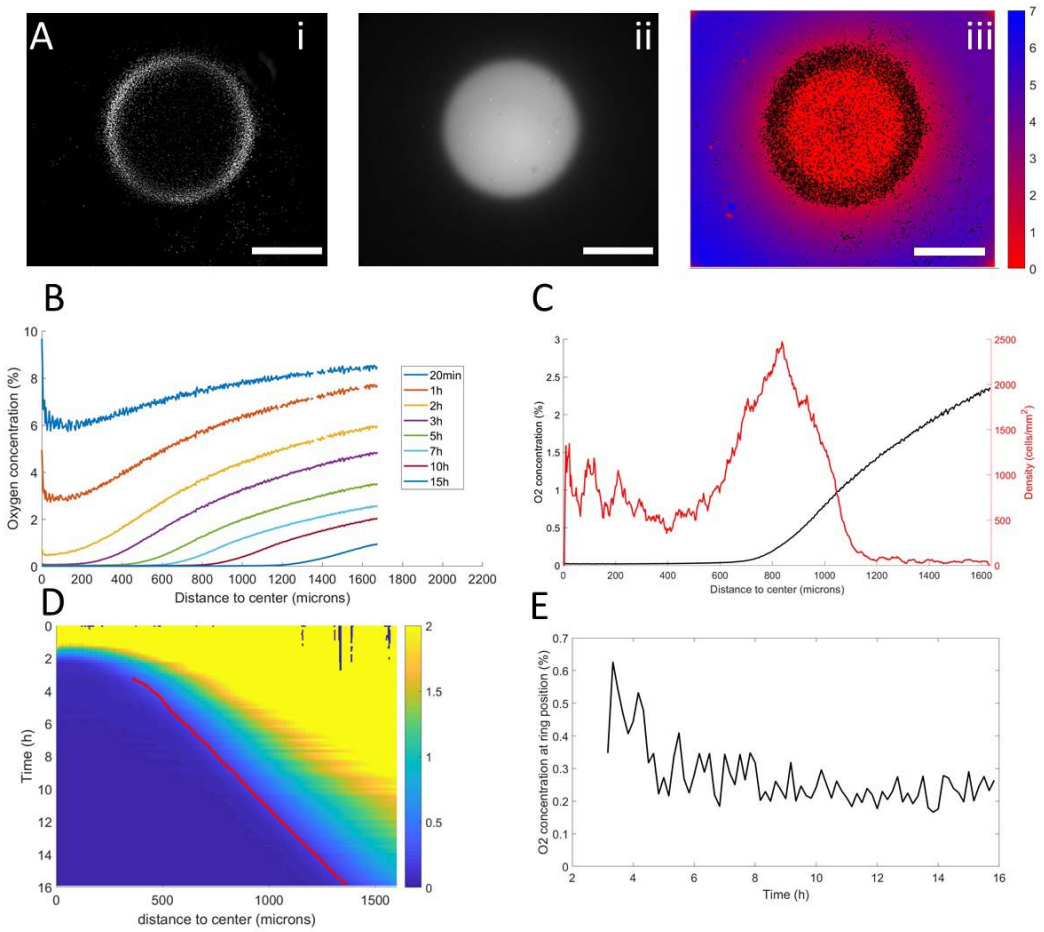

Fig3. *Interplay between ring dynamics and O_2 profiles. (A) i: treated image showing cell distribution at t=10h, ii: raw fluorescent signal indicative of strong O_2 depletion, iii: reconstructed image showing the center of mass of all detected cells and quantitative O_2 profiles (colorbar, in % of O_2), scale bars: 1mm.*

(B) O_2 profiles averaged over all angles and shown at different times. (C) radial profile of cell density and O_2 concentration at t=10h showing the position of the ring relative to the O_2 profile. (D) kymograph of O_2 concentration (colorbar in %) with the position of the ring represented as a red line. The colormap is limited to the 0-2% range for readability but earlier time points show concentrations higher than the 2% limit. (E) O_2 concentration as measured at the position of the ring as a function of time showing that the ring is indeed following a constant concentration after a transitory period.

Minimal cellular Potts Model. Based on these experimental results, we then asked whether this subtle response of *Dd* cells to complex oxygen environments was sufficient to explain the emergence of a highly stable, self-maintained collective phenomenon. To do so, we developed cellular Potts models based mostly on experimental observations and tested whether they could reproduce the observed cell dynamics. Briefly, the ingredient underlying the model are as follows (details can be found in the supporting information). First, all cells consume the oxygen that is locally available at a rate measured in (24). Cell activity (modelled here as an effective temperature) increases at low O_2. Cells also respond positively to O_2 gradients with a modulation of the strength of this aerotaxis based on local O_2 concentrations, as observed in our microfluidic experiments. Finally, all cells can divide. Of note, all parameters were scaled so that both time and length scales in the Potts models are linked to experimental times and lengths (see Supporting Information).

Although this model is based on experimental evidence, some of its parameters are not directly related to easily measurable biological properties. Therefore, we decided to fit our parameters to reproduce as faithfully as possible the results of our microfluidic experiments. However, to model the effect of a constant O_2 environment, consumption by cells was turned off in this fitting phase. Through a trial and error procedure, we managed to reproduce both qualitatively and quantitatively the results of the microfluidic experiments (Supplementary Movie M4) both in terms of collective behavior, in the form of cell accumulation, and individual cell behavior (Fig. S16).

We then applied this model and added O_2 consumption by cells, with initial conditions mimicking our spot assay and other ingredients mimicking the role of the confined geometry (see Supplementary Methods). We observed the rapid formation and migration of a high cell density ring (Fig. 4A-B, Supplementary Movie M5). This ring was remarkably similar to that observed in experiments. In particular, we found its speed to be constant after an initial transitory period (Fig. 4C, Fig. S17). This speed was also comparable to experimental ones. Similarly, the morphology of these simulated rings was constant over time with a fixed cell density and width (Fig. S17). Finally, cell behavior was qualitatively well reproduced by this model (Fig. S18) with the exception of a remaining dense core of cells in the center which disappeared if cell consumption (or initial cell density) was reduced (see Fig 5A).

In terms of coupled dynamics between cell density and O_2 profiles, we found here too that the driving force behind this collective phenomenon was the fact that the ring followed a constant O_2 concentration (Fig. 4D-E).

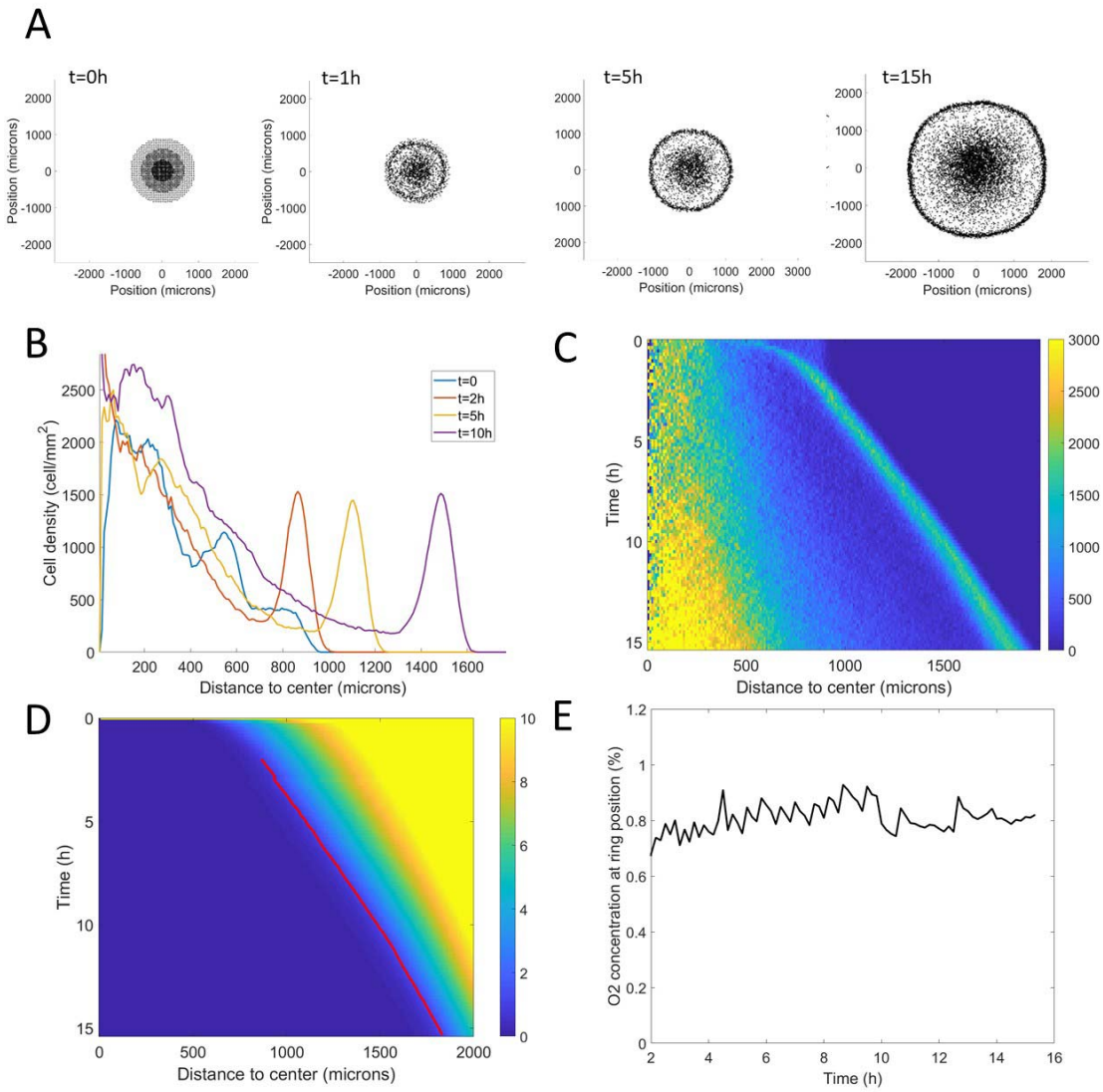

Fig. 4. Minimal Potts model of ring formation and migration. (A) Snapshots of a simulated colony of cells showing the formation of highly dense ring of cells. (B) Cell density profiles averaged over all angles for four different times. (C) Corresponding kymograph of cell density (colorbar in cells/mm^2) as a function of time and distance to the center. Quantification in terms of microns and hours is described in the supporting information. (D) Kymograph of O_2 concentration (colorbar in %) with the position of the ring represented as a red line. The colormap is limited to the 0-10% range for readability but earlier time points show concentrations higher than the 10% limit. (E) O_2 concentration at the ring position as a function of time showing that, here too, the ring follows a constant O_2 concentration.

Of note, these results show that the apparition of this collective phenomenon does not require any form of chemically-mediated communication between the cells unlike what was observed in the collective response of bacteria to self-generated gradients (25). We therefore asked what were the key ingredients in the model to trigger this seemingly collective phenotype, a question we explored by tuning our original Potts model. We started by dividing cell consumption of oxygen by a factor of 3 (Fig. 5A) and found that it didn't significantly change the ring speed but could change the aspect of cell density in the central region. We then turned our attention to other key elements in the model.

Cell division is crucial to the maintenance of a ring with constant morphology and increasing radius. Indeed, if we turned off cell division in our models, the formation of the ring was mostly unchanged but after a short time, the ring started slowing down and even stopped as cell density was no longer sufficient to reach highly hypoxic conditions (comparing Fig5 A and B). Second, we asked whether the observed and modelled aerokinesis was necessary to reproduce the collective migration. We found that it wasn't as models ran at different effective temperatures applied to all cells regardless of local O_2 concentrations, all showed qualitatively similar behavior (see for example Fig. 5C). Of note though, lower effective temperatures led to less dense rings as fewer cells were able to start in the ring (Fig. S19). Finally, we found that modulation of aerotaxis by local O_2 concentrations is essential. Indeed, as we increased the range of O_2 concentration at which aerotaxis is effective/at play, we found that forming rings became wider and less dense (Fig. 5 D-E) to the point where no actual ring could be distinguished if aerotaxis was kept constant for all cells (Fig. 5I).

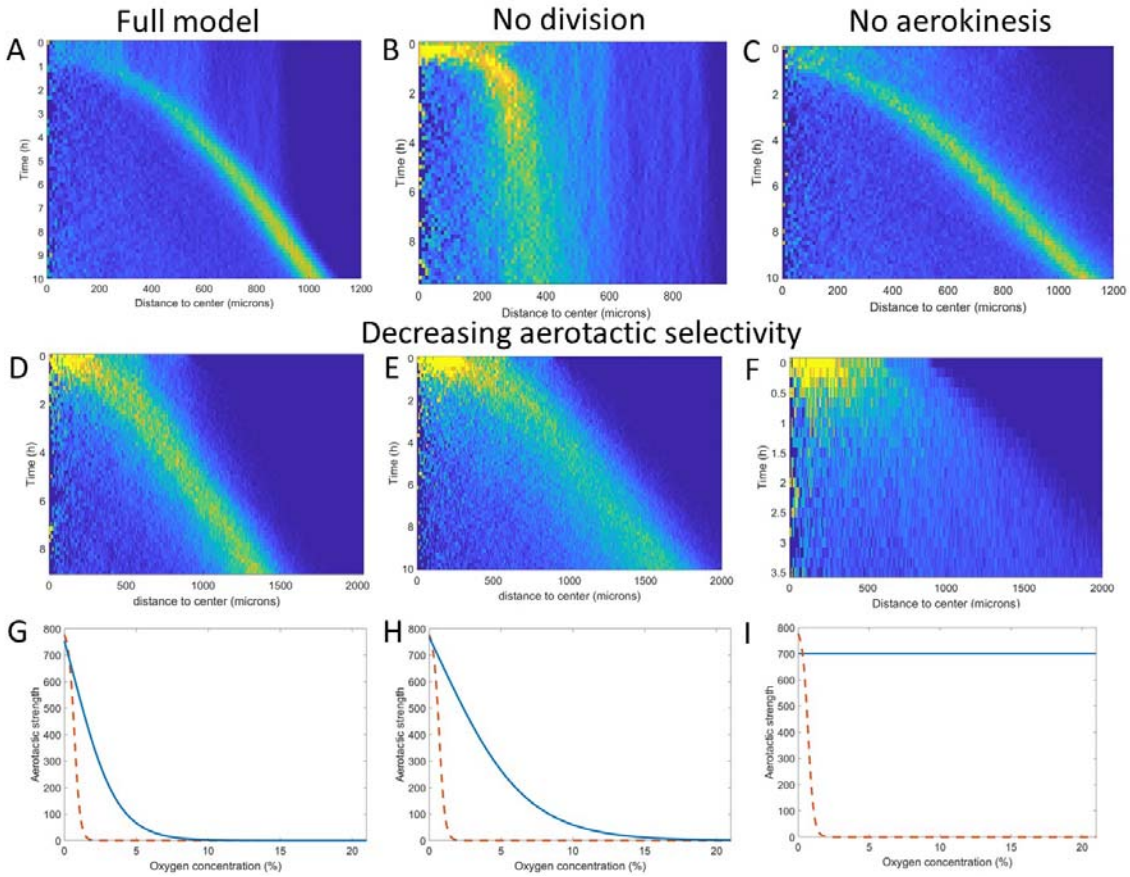

Fig. 5. *Key ingredients of the Potts model by density kymograph (DK) evaluation. (A) DK for the full model with reduced oxygen consumption as a basis for comparison. (B) DK in the absence of cell division, note the difference in length scale showing a clear limitation of motion in that case. (C) DK in the absence of aerokinesis (cell activity is not modulated by local oxygen concentrations). (D) DK with a modulation of aerotactic strength as shown in (G), note the wider ring. (E) DK with a modulation of aerotactic strength as shown in (H). (F) DK with a modulation of aerotactic strength as shown in (I), no ring appears and cells quickly migrate outwards as shown by the difference in time scales. (G-I) Three different aerotactic modulations, in blue, compared to the one used in the full model, shown in (A), drawn here as a red dashed line.*

These numerical simulations based on cellular Potts models provide a good intuition of the phenomenon and reveal that cell division and aerotactic modulation are the two key ingredients to

reproduce the formation and migration of a ring of cells. They fall short however of giving an in-depth quantitative description because they rely on many parameters and are not amenable to theoretical analysis *per se*.

Single-threshold 'Go or Grow' model. For the above mentionned reasons, we developed a simple, yet original, model based on the two key ingredients described above while keeping it analytically solvable. Cell density is treated as a continuous field, O_2 consumption and diffusion are included. Cells have two distinct behaviors, depending on the O_2 concentration. Below a certain threshold C_0 cells move preferentially upward the oxygen gradient, with constant advection speed a_0, but they cannot divide. Above the same threshold they can divide at constant rate and move randomly without directional bias. We refer to these two behaviors as respectively *go* or *grow*. We thereby revisit the 'Go or Grow' model for glioma cells introduced in (26), where the transition between proliferation and migration depends on the density of each phenotype, whilst here the transition between cell division and aerotactic motion is oxygen-mediated. This model is meant to 1- demonstrate that these ingredients are indeed sufficient to trigger a collective motion without signaling between cells and 2- determine the relative contributions of division and aerotaxis on the speed of the ring.

We restrict to the one-dimensional case for the sake of simplicity and because of its relevance for the analytical study of planar front propagation without curvature effects. Our simple 'Go or Grow' model is a piecewise constant reaction-advection-diffusion equation:

[EQ1]
$$\frac{\partial \rho}{\partial t} = D\frac{\partial^2 \rho}{\partial x^2} - \frac{\partial}{\partial x}\left(a(C)sign(\partial_x C)\rho\right) + r(C)\rho, with$$
$$a(C) = \begin{Bmatrix} 0\ if\ C > C_0 \\ a_0\ if\ C < C_0 \end{Bmatrix}$$
$$r(C) = \{\begin{matrix} r_0\ if\ C > C_0 \\ 0\ if\ C < C_0 \end{matrix}\}$$

$a(C)sign(\partial_x C)$ corresponds to the aerotactic advection speed and $r(C)$ to the cell division rate.

We assumed that the oxygen dynamics is subject to a simple diffusion-consumption equation, with b the constant consumption rate of oxygen per cell:

[EQ2]
$$\frac{\partial C}{\partial t} = D_{oxy}\frac{\partial^2 C}{\partial x^2} - b\rho C$$

The coupling goes through the location of the oxygen threshold switching between the two behaviors.

We investigated the existence of traveling wave profiles at some unknown speed $\sigma > 0$. The equation for the one-dimensional profile, being stationary in the moving frame $z = x - \sigma t$, is the following one:

[EQ3]
$$-\sigma\frac{\partial \rho}{\partial z} = D\frac{\partial^2 \rho}{\partial z^2} - \frac{\partial}{\partial z}\left(a(C)\rho\right) + r(C)\rho$$

Interestingly enough, it admits explicit solutions, whose speed does not involve the dynamics of oxygen consumption. This yields the following formula for the wave speed (Fig. 6A):

[EQ4]
$$\sigma = \begin{Bmatrix} a_0 + \frac{r_0 D}{a_0}\ if\ a_0 > \sqrt{r_0 D} \\ 2\sqrt{r_0 D}\ if\ a_0 \leq \sqrt{r_0 D} \end{Bmatrix}$$

This analytical formula is new up to our knowledge. It captures basic features of a wave under a single self-generated gradient.

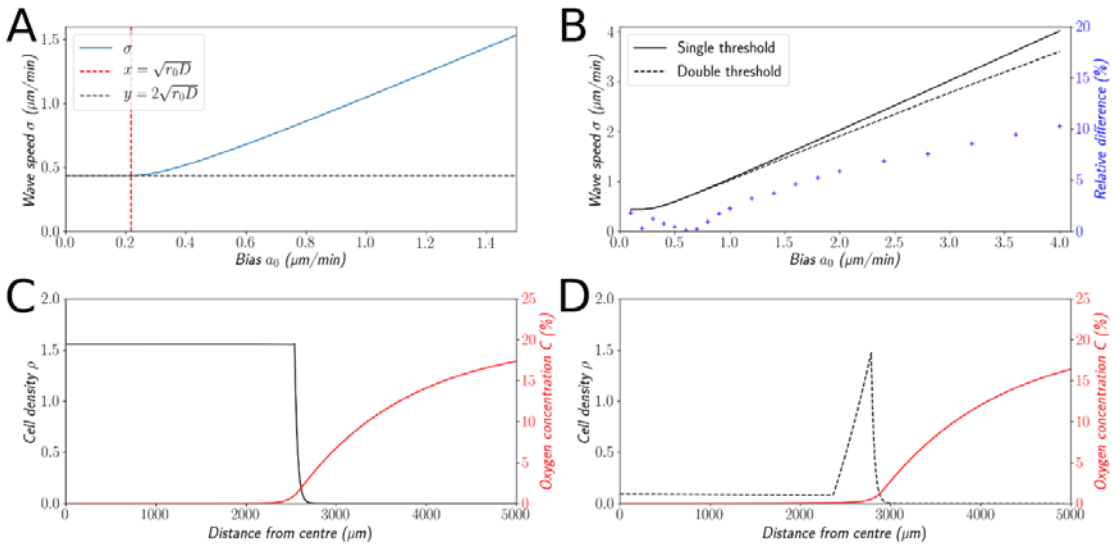

Fig. 6. *Simple 'Go or Grow' model. (A): Illustration of wave speed given by EQ4. (B): Comparison of wave speeds for the single-threshold and the double-threshold models (solid and dotted lines respectively) and relative difference between the two models (crosses). (C): Traveling wave profile of cell density and O_2 concentration for the single-threshold model (EQ1 & EQ2). (D): Traveling wave profile of cell density and O_2 concentration for the double-threshold model. In both cases, thresholds coincide with points of sharp transitions in the profiles.*

Double-threshold 'Go or Grow' model and variations. The monotonic cell density profile (Fig. 6C) of the 'Go or Grow' model EQ1 is clearly not in agreement with the observation of a dense ring of cells followed by an expanding zone at lower density (Fig. 1). Yet through elementary structural variations of the model, we obtained cell density profiles more similar to experimental ones, without significant alterations to the quantitative and qualitative conclusions.

First, we made the hypothesis of a second oxygen threshold , below which cells are not sensitive to gradients any longer. Notably, this model exhibits traveling wave profiles with a dense ring of cells, leaving behind a spatially uniform low cell density (Fig. 6D) much more similar to experimental observations. An exhaustive analytical investigation for this model seems out of reach, but the model can be analyzed numerically. The speed of the numerical wave remains close to the value given by formula EQ4 (at most 10% of relative difference for suitable parameters detailed in the supporting information, Fig. 6B). Intuitively, the main contribution to the collective speed is the strong bias inside the ring at intermediate levels of O_2, whereas cells at levels below the second threshold , where the dynamics of both models diverge, do not contribute much to the collective speed.

Second, we investigated more complex responses of cells to oxygen levels (Fig. S20). We assumed a continuous dependency of the bias to the O_2 concentration, rather than a discontinuous switch as in EQ1. In parallel, we assumed a continuous dependency of the division rate. The conclusions remain qualitatively and quantitatively the same (Fig. S20).

Therefore, properties of the 'Go or Grow' model EQ1, which we can prove analytically, like formula EQ4 and features discussed below, appear to be robust to substantial variations of the model.

Comparison with the Fisher-KPP reaction-diffusion equation. The Fisher-KPP equation is a standard model for the linear expansion of population range (27, 28). It describes front propagation under the combined effects of diffusion and growth. The wave speed of our 'Go or Grow' model coincides with Fisher's speed, i.e. in the regime of small bias ( ). This is the signature of a *pulled wave*, meaning that the propagation is driven by the division and motion of cells at the edge of the front, with negligible contribution from the bulk. In contrast, when the bias is large ( ) then the wave speed in [EQ4] is greater than Fisher's speed. This is the signature of a *pushed wave*, meaning that there is a significant contribution from the bulk to the net propagation.

In order to explore this dichotomy between pulled and pushed waves, we used the framework of neutral labeling introduced in (29) in the context of PDE models such as [EQ1]. We colored fractions of the initial density profile to mimic labeling of cells with two colors. Then, we followed numerically the dynamics of these fractions, and quantify the mixing of the two colors. Our results are in perfect agreement with (29), extending their results beyond classical reaction-diffusion equations, including advection (see supporting information section 3.2). In the case of large bias (Fig. 7A-C), where the migration does contribute to the wave speed, the wave is pushed and the profile is a perfect mixture of blue and yellow cells at long time, uniformly in space. Contrarily, the wave is pulled in the regime of small bias, where the directional migration does not contribute to the wave speed: only cells that were already initially in the front, here colored in blue (Fig. 7B-D), are conserved in the front, whilst yellow cells at the back cannot catch up with the front.

In the absence of associated experimental data, we explored the cellular Potts model with such neutral labeling. The results were in agreement with the PDE simulations (Fig. S21) showing a clear, rapid mixing of the two cell populations under the propagation of a pushed wave.

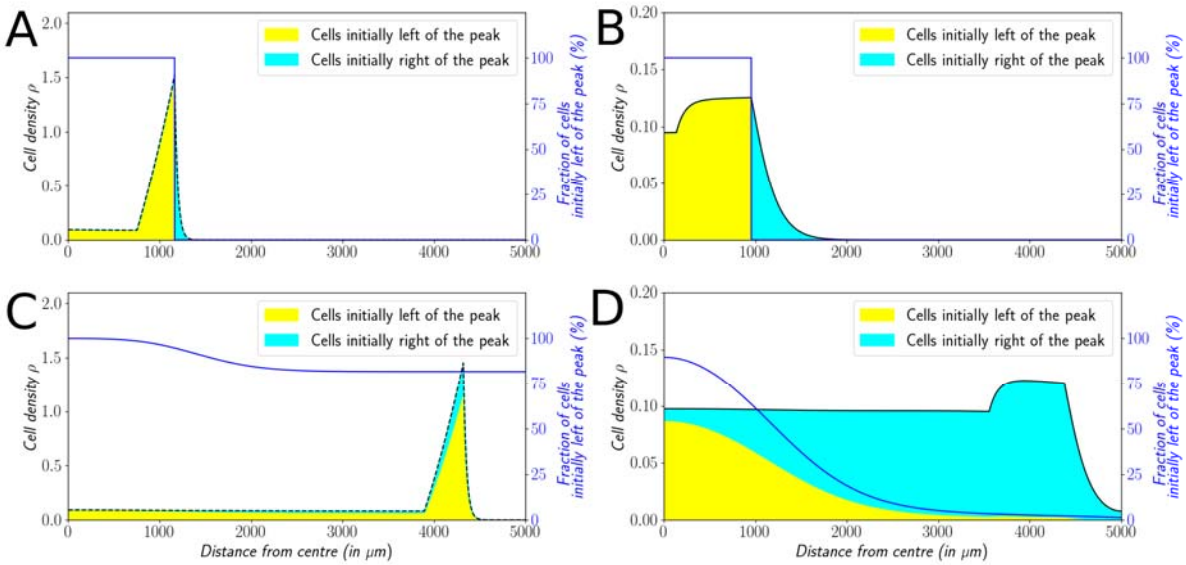

Fig. 7. *Classification of the expansion type. Cells initially on the left-hand side or right-hand side of the peak get labeled differently (A&B). The labeling is neutral and does not change the dynamics of the cells. We let evolve the two colored population for some time and observe the mixing of the colors (C&D). (A&C) : With , the wave is pushed wave and after some time the front*

undergoes a spatially uniform mixing. (B&D) : With $a_0 = 0.1\mu m \cdot s^{-1}$, the wave is pulled and only the fraction initially in the front is conserved in the front.

Relative contribution of growth and aerotactic bias to the collective motion in experiments. In [EQ4] we see that growth contributes to the wave speed either, as for the standard Fisher reaction-diffusion model, via the geometric mean of growth rate $r_0$and diffusion coefficient D, in the case of small bias ($a_0 \sqrt{r_0 D}$), or via a linear term supplementing the advection speed $a_0$for large bias ($a_0 > \sqrt{r_0 D}$). As a rough approximation with $a_0 = 1\mu m \cdot min^{-1}$ in experiments, assuming a doubling time of 8h for *Dd* cells, $r_0 = ln\, 2/480\, min^{-1}$and $D = 30\mu m^2 \cdot min^{-1}$, we are clearly in the case of large bias ($\sqrt{r_0 D} = 0.21\mu m \cdot min^{-1}$) and EQ4 yields $\sigma = 1.04\mu m \cdot min^{-1}$. The exact contribution of growth depends on the variations of the model (numerical explorations have shown contributions of growth of at most 20%, see Supporting Information), yet even with this elementary reasoning we were able to estimate that growth contributes only up to a small fraction to the overall speed.

Noticeably, there is an alternative viewpoint that combines the shape of the density profile and the wave speed. By integrating [EQ3] over the line, we obtain

[EQ3bis] $$\Big(\sigma - a\big(C(-\infty)\big)\Big)\rho(-\infty) = \int r\big(C(z)\big)\rho(z)dz$$

This equation balances the net flux of cells to the far left-hand with the amount of mass created by heterogeneous (signal-dependent) cell division.

Formula [EQ3bis] remains true under variations of the simple 'Go or Grow' model, as it merely results from mass balance. We illustrate this relationship with the experimental data from Fig. 1E. We approximate the area under the curve by a rectangle method: $\int r\big(C(z)\big)\rho(z)dz = r_0\hat{\rho}L$ where L is the length spanned by the ring and $\hat{\rho}$ is the average cell density in the ring. As there is supposedly no advection $a(C) = 0$ at $z = -\infty$ this yields the approximation $\sigma \approx \frac{r_0 L\hat{\rho}}{\rho(-\infty)}$. Quantitatively, we assume L to be on the order of 300µm (Fig. 1E) and $\frac{\hat{\rho}}{\rho(-\infty)}$, the ratio between cell densities in the ring and in the bulk of cells, to be on the order of 4 (Fig. 1E). This yields an estimate of the wave speed of $\sigma \approx 1.7\mu m.min^{-1}$ relatively similar to the estimate given by [EQ4]. Overall, the invesvestigations of the 'Go or Grow' model and its variations show that the ring speed is mainly the outcome of the interplay between cell division and aerotaxis.

Discussion

Oxygen is present everywhere on earth's surface. In living matter, the local O_2 concentration results from the balance between molecular diffusion across tissues from O_2 sources (such as blood or external atmosphere) and the local O_2 consumption such as cell respiration. While aerotaxis is well established for bacteria, its role is often invoked in multicellular organisms to explain various processes in development or cancer progression, but very few *in vitro* studies were conducted to prove it is an efficient and operating mechanism or to understand the molecular mechanisms at play during aerotaxis.

Deygas et al. showed that confined epithelial colonies may trigger a self-generated O_2 gradient and an aerotactic indirect response through a secondary ROS self-generated gradient (9). Gilkes et al. showed that hypoxia enhances MDA-MB231 breast cancer cell motility through an increased activity of hypoxia-inducible factors (HIFs) (30). HIFs activate transcription of the Rho family member RHOA and Rho kinase 1 (ROCK1) genes, leading to cytoskeletal changes, focal adhesion formation and

actomyosin contractions that underlie the invasive cancer cell phenotype. This study suggests a role for aerotaxis in tumor escape, but it only demonstrates aerokinesis as O_2 gradients were not imposed to probe a directed migration toward O_2. Using a microfluidic device, the same cancer cell line was submitted to various oxygen levels as well as oxygen gradients (31). An enhanced activity was observed around 5% O_2 but observed aerotactic response was not clear. Note that no change in mesenchymal cell motility was observed during the first 14 h of incubation at 1% O_2 with MDA-MB231 cells on stiff surfaces, but cell motility increased after that time. Immunoblot assays of MDA-MB-231 lysates confirmed that RhoA and ROCK1 induction occurs at 12 h and is maintained through 48 h of hypoxic exposure (30).

By contrast, the experimental results presented here with *Dd* show a very quick response to hypoxia. Cells exhibit within 15 min an aerokinetic (enhanced speed) and aerotactic (directed migration towards O_2) response when exposed to externally imposed O_2 gradients created by microfluidic devices (Fig. 2). Self-generated O_2 gradients are produced within 20 min (Fig. 3 and Fig. S2). But this cellular response is within the equilibration time of the oxygen distribution (Fig. S14). Hence we can consider the cellular response as almost instantaneous with *Dd*. The difference with MDA-MB231 cells is probably due to the extreme plasticity of the rapidly moving amoeboid cells (*Dd*) and their almost adhesion independent migration mechanism (32) while mesenchymal cancer cells move slower by coordinating cytoskeleton forces and focal adhesion (33).

The quick response of *Dd* in directed migration assays has been largely exploited to decipher the molecular mechanisms at play during chemotaxis (34). The molecular mechanisms used for O_2 sensing and its transduction into cellular response are for the moment unknown but we can expect that the O_2 molecular sensors modulate cytoskeleton organization, particularly localized actin polymerization/depolymerization through some of the molecular components involved in classical chemotaxis toward folate or cAMP (35, 36). However, new and unexpected mechanisms cannot be excluded.

The finding that migrating cells can influence the direction of their own migration by building chemoattractant gradients is not new but it was only recently reported for various systems (10): melanoma cells that break down lysophosphatidic acid (LPA) and generate a LPA gradient in the vicinity of the tumor (11), *Dd* colonies that generate folate gradients (12) or for the migration of the zebrafish lateral line primordium through a self-generated chemokine gradient (13, 14). The dispersal of melanoma cells is particularly instructive. The stroma surrounding the tumor acts as a source of LPA. The tumor cells act as a sink for LPA. As long as LPA is present in the environment, after a quick transient, a steady wave of migrating melanoma cells propagates away from the initial tumor over long distances and long time periods.

The self-generated LPA (melanoma) and folate (*Dd*) gradients were modeled with a simple numerical model that was able to predict the steady wave. In particular, it predicted an invasive front where cells are exposed to a steep chemoattractant gradient, followed by a 'trailing end' where the gradient is shallow and fewer cells migrate with poor directionality (37). It also predicted that the wave may have a less marked front, and/or a smaller speed, or even vanishes if the cell density was too low due to insufficient chemoattractant removal. All these features are surprisingly similar to our experimental measurements of cell density and O_2 profiles (Fig. 1E, Fig. 3C). The atmospheric O_2 that diffuses through the culture medium and eventually the plastic surfaces is the chemoattractant. The O_2 consumption triggers hypoxia that in turn generate an aerotactic response toward O_2 in a very narrow range of O_2 concentrations (~0.1-1.5%) (Fig. 3C). The exact value of the lower O_2 threshold value (*i.e.*, 0.1%) is taken from the error bar on the O_2 measurement in that range (inset of Fig. S11H) but will deserve future investigations. The exact nature of the cellular response at these extremely low O_2 levels, and in a very shallow gradient, has yet to be clarified experimentally.

Our different models unveil a set of basic assumptions which are sufficient for collective motion of cells without cell-cell interactions (attractive or otherwise), in contrast with (25). Cell growth is necessary to produce a long-standing wave without any damping effect. However, it may not be the main contribution in the wave speed, depending on the relative ratio between directional motion (the bias a_0), and reaction-diffusion (the Fisher half-speed $\sqrt{r_0 D}$). In the case where the former is greater than the latter, the wave is due to the combination of growth and directional motion and it is

pushed (significant contribution of the bulk to the propagation). This result differs particularly from the Fisher equation with constant advection (meaning with uniform migration and division) where the wave speed is $a_0 + 2\sqrt{r_0 D}$ and the wave is pulled (significant contribution of the edge of the front). In the experiments under study, we estimate directional motion to contribute the most to the cell speed, ruling out the possibility of seeing a pulled wave driven by cell division and diffusion at the edge of the front.

In conclusion, we demonstrate the remarkable stability of collective motion driven by self-generated gradients through depletion of an attractant. Through coupled dynamics, these gradients give rise to long lasting, communication-free migrations of entire colonies of cells which are important both from ecological and developmental points of view. In the case presented here where oxygen plays the role of the depleted attractant, this could prove to be a very general mechanism as oxygen is ubiquitous and always consumed by cells.

Material and methods

Cell preparation. Cells were grown in HL5 media at 22°C with shaking at 180 rpm for oxygenation (38). Exponentially growing cells were harvested, counted to adjust cell density at typically 2000 cells/µL. For the spot assay, 1 µL of cell suspension was carefully deposited on a dry surface (6 wells plastic plates or PDMS for oxygen sensing) and incubated for 5 to 7 minutes in humid atmosphere. 2 ml HL5 was slowly added to avoid detaching cells and a wetted coverslip was then deposited on top of the micro-colony. The micro-colony was then observed under video-microscope and analysed with ImageJ and Matlab (see supporting information).

Microfluidic devices and O_2 sensing films. Using soft lithography, we manufactured a double layer PDMS microfluidic device to control a O_2 gradient along the cell-media channel. The gradient is established within 15 min. We also developed coverglass coated with a thin layer of PDMS with porphyrin embedded: the quenching by O_2 of the porphyrin luminescence enables the direct measurement of the O_2 concentration from a proper calibration of the fluorescence intensity (details are given in the supporting information).

Potts models. Potts model simulations were run using CompuCell3D (39) with a mix of prebuilt modules and home-made Python steppables in particular to implement the modulation of aerotactic strength by local oxygen levels. Most parameters were fitted to experimental measurements and both time and length scales were also adapted to achieve quantitative simulations. Full details of the model can be found in Supplementary Methods and full codes are available upon request to the corresponding authors.

Go or grow model and simulations. Both diffusion equations EQ1&EQ2 were discretized through a time-backward space-centered difference scheme with an upwind discretization for the advection operator:

$$\frac{\rho_i^{n+\frac{1}{2}}-\rho_i^{n-\frac{1}{2}}}{\Delta t} - D\,\frac{\rho_{i-1}^{n+\frac{1}{2}}-2\rho_i^{n+\frac{1}{2}}+\rho_{i+1}^{n+\frac{1}{2}}}{\Delta x^2} + \frac{1}{\Delta x}\cdot\left\{\begin{matrix} a_i^n\rho_i^{n+\frac{1}{2}} - a_{i-1}^n\rho_{i-1}^{n+\frac{1}{2}} if C_i^n \geq C_{i-1}^n \\ a_i^n\rho_i^{n+\frac{1}{2}} - a_{i+1}^n\rho_{i+1}^{n+\frac{1}{2}} if C_i^n < C_{i-1}^n \end{matrix}\right\} = r_i^n\rho_i^{n+\frac{1}{2}}, \text{ where}$$

$$a_i^n = a(C_i^n), r_i^n = r(C_i^n)$$

$$\frac{C_i^{n+1}-C_i^n}{\Delta t} - D_{oxy}\frac{C_{i-1}^{n+1}-2C_i^{n+1}+C_{i+1}^{n+1}}{\Delta x^2} = -b\rho_i^{n+\frac{1}{2}}C_i^{n+1}$$

The schemes were coded in Python language. All simulations of EQ1&EQ2 shown in this article were carried out with a mesh size $\Delta t = 1min$ and $\Delta x = 1\mu m$. The values used for the constants are : $D = 30\mu m^2 \cdot min^{-1}$, $C_0 = 1\%$, $C_0{}' = 0.1\%$, $D_{oxy} = 1300\mu m^2 \cdot s^{-1}$, $r_0 = log\ 2/480\ min^{-1}$and $b = 0.1\ O_2\%min^{-1}cell^{-1}$.

Acknowledgments

We thank P. Gonzalo and I. Mikaélian for fruitful initial discussions on aerotaxis; R. Fulcrand for his expert help in microfabrication; G. Torch, C. Zoude, G. Simon and A. Piednoir for technical assistance. We would like to thank the *Dictyostelium* Stock Centre hosted at the Northwestern University for the SodA overexpression line. This study was supported by the CNRS - Mission pour les Initiatives Transverses et Interdisciplinaires – « Défi Modélisation du vivant - 2019 », by the GDR ImaBio (AMI fellowship) and by the IFS LyC Collaborative Research Project 2019 (Tohoku University). S. Hirose was supported by the STARMAJ Program (France-Japan: Research Internships for Master's Students, Université de Lyon) and K. Funamoto by the CNRS (invited researcher position). This project has received funding from the European Research Council (ERC) under the European Union's Horizon 2020 research and innovation programme (grant agreement No 639638 to V. Calvez).

References

1. X. Chen, *et al.*, Rise to modern levels of ocean oxygenation coincided with the Cambrian radiation of animals. *Nat. Commun.* **6**, 7142 (2015).

2. F. Tonon, *et al.*, In vitro metabolic zonation through oxygen gradient on a chip. *Sci. Rep.* **9**, 13557 (2019).

3. C. W. Pugh, P. J. Ratcliffe, New horizons in hypoxia signaling pathways. *Exp Cell Res* **356**, 116–121 (2017).

4. T. W. Engelmann, Neue methode zur untersuchung der sauerstoffausscheidung pflanzlicher und tierischer organismen (New method for investigation of oxygen-searching plant and animal organisms). *Pflugers Arch. Gesammte Physiol.* **25**, 285–292 (1881).

5. K. M. Winn, D. G. Bourne, J. G. Mitchell, Vibrio coralliilyticus Search Patterns across an Oxygen Gradient. *PLoS One* **8**, 1–8 (2013).

6. T. W. Lyons, C. T. Reinhard, N. J. Planavsky, The rise of oxygen in Earth's early ocean and atmosphere. *Nature* **506**, 307–315 (2014).

7. O. Genbacev, Y. Zhou, J. W. Ludlow, S. J. Fisher, Regulation of human placental development by oxygen tension. *Science (80-.).* **277**, 1669–1672 (1997).

8. D. M. Lewis, *et al.*, Intratumoral oxygen gradients mediate sarcoma cell invasion. *Proc. Natl. Acad. Sci. U. S. A.* **113**, 9292–7 (2016).

9. M. Deygas, *et al.*, Redox regulation of EGFR steers migration of hypoxic mammary cells towards oxygen. *Nat. Commun.* **9**, 4545 (2018).

10. C. H. Stuelten, Moving in and Out: Dispersion of Cells in Self-Generated Gradients. *J. Clin. Cell. Immunol.* **08** (2017).

11. A. J. Muinonen-Martin, *et al.*, Melanoma Cells Break Down LPA to Establish Local

Gradients That Drive Chemotactic Dispersal. *PLoS Biol.* **12** (2014).

12. L. Tweedy, O. Susanto, R. H. Insall, Self-generated chemotactic gradients - cells steering themselves. *Curr. Opin. Cell Biol.* **42**, 46–51 (2016).

13. E. Donà, *et al.*, Directional tissue migration through a self-generated chemokine gradient. *Nature* **503**, 285–289 (2013).

14. G. Venkiteswaran, *et al.*, Generation and dynamics of an endogenous, self-generated signaling gradient across a migrating tissue. *Cell* **155**, 674 (2013).

15. D. A. Cotler, K. B. Raper, Properties of Germinating Spores of Dictyostelium discoideum. *J. Bacteriol.* **96**, 1680–1689 (1968).

16. D. Sandonà, S. Gastaldello, R. Rizzuto, R. Bisson, Expression of Cytochrome c Oxidase during Growth and Development of Dictyostelium. *J. Biol. Chem.* **270**, 5587–5593 (1995).

17. Y. Xu, Z. A. Wang, R. S. Green, C. M. West, Role of the Skp1 prolyl-hydroxylation/glycosylation pathway in oxygen dependent submerged development of Dictyostelium. *BMC Dev. Biol.* **12** (2012).

18. R. H. Kessin, *Dictyostelium: evolution, cell biology, and the development of multicellularity.* (Cambridge University Press, 2001).

19. P. Pan, E. M. Hall, J. T. Bonner, Folic acid as second chemotactic substance in the cellular slime moulds. *Nat. New Biol.* **237**, 181–182 (1972).

20. E. F. Keller, L. A. Segel, Initiation of slime mold aggregation viewed as an instability. *J. Theor. Biol.* **26**, 399–415 (1970).

21. T. Hillen, K. J. Painter, A user's guide to PDE models for chemotaxis. *J. Math. Biol.* **58**, 183–217 (2009).

22. H. Delanoë-Ayari, *et al.*, Changes in the magnitude and distribution of forces at different dictyostelium developmental stages. *Cell Motil. Cytoskeleton* **65**, 314–331 (2008).

23. B. Ungerböck, V. Charwat, P. Ertl, T. Mayr, Microfluidic oxygen imaging using integrated optical sensor layers and a color camera. *Lab Chip* **13**, 1593–601 (2013).

24. P. Torija, *et al.*, Functional genomics in Dictyostelium: MidA, a new conserved protein, is required for mitochondrial function and development. *J. Cell Sci.* **119**, 1154–1164 (2006).

25. J. Saragosti, *et al.*, Directional persistence of chemotactic bacteria in a traveling concentration wave. *Proc. Natl. Acad. Sci.* **108**, 16235–40 (2011).

26. H. Hatzikirou, D. Basanta, M. Simon, K. Schaller, A. Deutsch, "Go or grow": The key to the emergence of invasion in tumour progression? *Math. Med. Biol.* **29**, 49–65 (2012).

27. R. A. Fisher, The wave of advance of advantageous genes. *Ann. Eugen.* **7**, 355–369 (1937).

28. A. Kolmogorov, I. Petrovskii, N. Piskunov, Etude de l'équation de la diffusion avec croissance de la quantité de matière et son application à un problème biologique.

Bull. Univ. Moskow, Ser. Internat., Sec. A **1**, 1–25 (1937).

29. L. Roques, J. Garnier, F. Hamel, E. K. Klein, Allee effect promotes diversity in traveling waves of colonization. *Proc. Natl. Acad. Sci. U. S. A.* **109**, 8828–8833 (2012).

30. D. M. Gilkes, *et al.*, Hypoxia-inducible factors mediate coordinated RhoA-ROCK1 expression and signaling in breast cancer cells. *Proc. Natl. Acad. Sci. U. S. A.* **111**, E384 (2014).

31. R. Koens, *et al.*, Microfluidic platform for three-dimensional cell culture under spatiotemporal heterogeneity of oxygen tension. *APL Bioeng.* **4**, 016106 (2020).

32. P. Friedl, S. Borgmann, E. B. Bröcker, Amoeboid leukocyte crawling through extracellular matrix: lessons from the Dictyostelium paradigm of cell movement. *J. Leukoc. Biol.* **70**, 491–509 (2001).

33. S. P. Palecek, J. C. Loftust, M. H. Ginsberg, D. A. Lauffenburger, A. F. Horwitz, Integrin-ligand binding properties govern cell migration speed through cell-substratum adhesiveness. *Nature* **385**, 537–540 (1997).

34. A. Nakajima, S. Ishihara, D. Imoto, S. Sawai, Rectified directional sensing in long-range cell migration. *Nat. Commun.* **5**, 1–14 (2014).

35. M. Pan, X. Xu, Y. Chen, T. Jin, Identification of a Chemoattractant G-Protein-Coupled Receptor for Folic Acid that Controls Both Chemotaxis and Phagocytosis. *Dev Cell.* **36**, 428–439 (2016).

36. P. J. M. Van Haastert, I. Keizer-Gunnink, A. Kortholt, Coupled excitable Ras and F-actin activation mediates spontaneous pseudopod formation and directed cell movement. *Mol. Biol. Cell* **28**, 922–934 (2017).

37. L. Tweedy, R. H. Insall, Self-Generated Gradients Yield Exceptionally Robust Steering Cues. *Front. Cell Dev. Biol.* **8** (2020).

38. M. Sussman, Cultivation and Synchronous Morphogenesis of Dictyostelium under Controlled Experimental Conditions. *Methods Cell Biol.* **28**, 9–29 (1987).

39. M. H. Swat, *et al.*, "Chapter 13 – Multi-Scale Modeling of Tissues Using CompuCell3D" in *Methods in Cell Biology*, (2012), pp. 325–366.